BNL-67805

AN INVESTIGATION OF THE EFFECT OF SULFATE ON CLOUD MICROPHYSICS USING A CHEMISTRY/TRANSPORT MODEL

Harshvardhan, D. Wei, and R. Green
Purdue University
West Lafayette, Indiana

S. E. Schwartz and C. M. Benkovitz
Brookhaven National Laboratory
Upton, NY 11973-5000

September 2000

For publication in preprint volume
Millennium Symposium on Atmospheric Chemistry:
Past, Present, and Future of Attmospheric Chemistry, 14-19 January 2001,
Albuquerque, NM, Paper No. 6.5, American Meteorological Society, Boston, MA.

Research by BNL investigators was performed under the auspices of the U.S. Department of Energy under Contract No. DE-AC02-98CH10886.

6.5 AN INVESTIGATION OF THE EFFECT OF SULFATE ON CLOUD MICROPHYSICS USING A CHEMISTRY/TRANSPORT MODEL

Harshvardhan*, Dongjiao Wei and Robert Green
Purdue University, West Lafayette, Indiana

Stephen Schwartz and Carmen Benkovitz
Brookhaven National Laboratory, Upton, New York

1. INTRODUCTION

It is now generally accepted that a complete picture of anthropogenic radiative forcing of the earth system requires the consideration of aerosols. Aerosol radiative forcing is typically classified as being direct – an increase (usually) in system albedo caused by the additional atmospheric optical depth, or indirect – an increase of cloud droplet number concentration leading to an increase in system albedo (Twomey, 1977). These forcings together are potentially of the same order of magnitude as greenhouse gas forcing but have opposite sign (IPCC 1995). Although the magnitude of both aerosol radiative forcings on a global scale is quite uncertain, the study of indirect radiative forcing is particularly problematic because it involves subtle changes in cloud radiative properties and lifetimes.

Studies to date have typically been limited to *in-situ* characterization of cloud microphysics, such as comparison of marine and polluted air (Brenguier et al. 2000) or global satellite surveys showing mean differences in hemispheric and continental/maritime clouds (Han et al. 1994). In this study we investigate the effect of aerosol on low-level clouds in a synoptic framework. The study of cloud processes is best accomplished by *in-situ* investigations but these are prohibitively expensive to conduct on anything close to a global scale. The standard solution to this dilemma is to resort to remote sensing procedures anchored by limited *in-situ* results. Unfortunately, aerosols cannot be detected remotely in the presence of cloud so their interaction cannot be studied solely from remote instrumentation.

Here we adopt a hybrid method to study the problem. We use the sulfate column burden simulated by an aerosol chemical transport model as an indicator of aerosol concentration. Cloud microphysics is inferred remotely from AVHRR Global Area Coverage (GAC) data over the North Atlantic. Information from the two sources is combined to assess the potential of aerosol indirect radiative forcing.

2. CHEMICAL TRANSPORT MODEL

The Brookhaven National Laboratory (BNL) chemical transport and transformation model, the **G**lobal **Ch**emistry **M**odel driven by **O**bservation-derived synoptic meteorological data (GChM-O), is described in Benkovitz et al. (1994) and Benkovitz and Schwartz (1997). The model, a three-dimensional Eulerian transport and transformation model, is driven by synoptic meteorological data assimilated from observations. The model represents emissions of the several sulfur species, chemical conversion of SO_2 to sulfate by H_2O_2 and O_3 in the aqueous phase and by OH in the gas phase, chemical conversion of DMS to SO_2 and MSA by OH, and removal by wet and dry deposition. The model tracks the several sulfur species according to the source type and region and conversion mechanism. The model has a horizontal grid spacing of 1.125 latitude × 1.125 longitude, 15 levels to 100 hPa and outputs the mixing ratios of SO_2 and sulfate at each grid cell location and model level at 6-hour time intervals.

Output of a model run for April 1987 was used to identify a time period for investigating the indirect radiative effect of anthropogenic aerosols in the North Atlantic. During early April the eastern North Atlantic came under the influence of a cut-off low-pressure system that transported boundary layer air from source regions in northwestern Europe (Benkovitz et al. 2001). We focus here on the period April 2-8. The model output shows that a mass of relatively polluted air from Northern Europe invaded the area from the east after April 3 and that the region again became relatively clean by April 8. Figure 1 shows the column burden of sulfate simulated by GChM-O on April 2 and April 5, both at 1800 UTC. Within the region, we have chosen the area bounded by longitudes 25W and 30W and latitudes 50N and 55N to investigate changes in cloud microphysics over the time period. This area is indicated in the figure and is henceforth referred to as Region A. As we wish to examine the relation between cloud microphysical properties and the intrusion of sulfate aerosol from Europe it is necessary to minimize other sources of aerosol such as desert dust or organics from biomass burning. Restricting the analysis to the higher latitudes reduces the possibility of contamination, although it probably does not eliminate it altogether.

3. REMOTELY SENSED DATA

For this study we have obtained cloud microphysical information from a two-channel method using AVHRR GAC data (Nakajima and Nakajima 1995). The procedure makes use of Channels 1 (visible), 3 (near-infrared) and 4 (infrared window) to obtain cloud droplet effective radii and cloud optical depth for each pixel. As

Corresponding author address: Harshvardhan, Purdue Univ., Dept. of Earth & Atmospheric Sciences, West Lafayette, IN 47907-1397; e-mail: harsh@purdue.edu.

the inversion process is based on plane-parallel radiative transfer and an assumption of horizontal homogeneity, caution must be used in selecting pixels for processing and interpreting results. For this study, we have restricted ourselves to oceanic regions, so the background albedo is low and homogeneous. Furthermore, we have used a lower cutoff of 0.10 in Channel 1 albedo to eliminate pixels that could be covered by haze but not clouds.

GAC pixels are roughly 4 × 1 km at nadir, and hence there is a good chance that they are not completely covered by clouds. Partially filled pixels will bias the inferred retrievals of effective radius and optical depth. One way around this problem is to use a high threshold for the visible channel, say 0.40, which should eliminate most partially filled pixels. However, this also eliminates many cloud-covered pixels for which information should be included and restricts the analysis to the thicker portions of the cloud field. In this study we have opted for the screening technique pioneered by Coakley and Bretherton (1982) – the spatial coherence method. Although used initially for higher resolution Local Area Coverage (LAC) data in regions with primarily single layered low clouds, the method has also been applied to GAC data (Coakley and Davies 1986), and we have used the local standard deviation of Channel 4 radiance in 2 × 2 pixel arrays to screen out partially cloud-filled pixels.

3.1 *Spatial Coherence Screening*

Figure 2 shows two panels from April 2 and 5, respectively, in which the local standard deviation in radiance units is plotted versus the mean radiating temperature of 2 × 2 pixel arrays for all pixels in Region A. Satellite overpass times for this region vary from 1630 to1600 UTC over the course of the period of study. As GAC data samples every third scan line and skips one pixel in five while averaging along a scan line, the array represents an area of 9 × 4 km at nadir. Low values of the standard deviation indicate homogeneity on that scale. The two "feet" of the "arch" in the left hand panel correspond to the clear ocean surface (278-280 K) and tops of cloud filled pixels (260-262 K). Although the same features are present on April 5, the scatter at temperatures colder than the "foot" at 270 K indicates high broken clouds. Judiciously choosing an upper limit for the standard deviation and lower limit for radiating temperature, restricts our analysis to those pixels that are most probably covered completely by clouds consisting of water droplets.

Figure 3 shows an analysis of the April 2 case in which the cloud optical depth has been retrieved for all pixels (upper left panel), and for progressively tighter restrictions on the local standard deviation of Channel 4 radiance. Each dot in the scatter plot of Figure 2 corresponds to four pixels that have passed the standard deviation test. The retrieved optical depth is plotted against the inferred cloud-top temperature, one of the output fields of the inversion procedure, produced by using the Channel 4 radiance, the sea-surface temperature and cloud transmittance. This temperature is typically a little colder than the Channel 4 radiating temperature. The sharp cutoff at an optical depth of about 2, clearly evident in the top two panels, is a result of the Channel 1 albedo threshold of 0.10. As the standard deviation threshold is applied, numerous pixels with warm radiating temperatures are screened out, leaving those that are most probably cloud-filled when the threshold is 0.5 mW m^{-2} sr^{-1} cm. This procedure therefore allows inclusion of a full range of retrieved optical depths and effective droplet radii (not shown) for cloud-filled pixels while at the same time reduces biases that would appear if all pixels were analyzed. A comparison of the upper left and lower right panels illustrates quite dramatically the potential for making incorrect inferences regarding the distribution of cloud optical depths for this case. For the rest of the analysis, only those pixels having Channel 4 local standard deviation < 0.5 mW m^{-2} sr^{-1} cm and Channel 4 local mean radiating temperature > 260 K are considered.

4. CLOUD MICROPHYSICS

The two directly inferred cloud properties from the inversion procedure are effective droplet radius, r_e, and cloud optical depth, τ. The effective radius is a measure of the droplet size at some distance just below the top of the cloud, averaged horizontally over the entire pixel. The optical depth is also an effective radiance-weighted measure representative of the pixel. Two additional microphysical quantities can be derived from r_e and τ. The liquid water path, LWP (g/m^2), is an integrated measure of the total condensed water in a vertical column extending from the base of the cloud to the top and is approximated by (Stephens 1984)

$$LWP = (2/3)\, \rho_w\, \tau\, \langle r_e \rangle. \qquad (1)$$

Furthermore, the column droplet concentration, N_c (number/cm^2), which is the vertical integral of the droplet number concentration, can be expressed as (Han et al. 1998)

$$N_c = (3\ LWP) / (4\, \pi\, \rho_w \langle r_v^3 \rangle) \qquad (2)$$

In the above, angle brackets denote a vertical average through the cloud, ρ_w is the density of liquid water and r_v is the volume-mean droplet radius. As the reflected radiance measured remotely does not provide information from deeper regions of the cloud, some assumptions need to be made in order to obtain a column-mean effective radius. We follow Brenguier et al. (2000) and assume that $\langle r_e \rangle = 5/6\ r_e$. The droplet spectral shape determines the ratio $k = r_v^3/r_e^3$; here we choose k = 0.735, which is the midpoint of the range quoted by various investigators (Brenguier et al. 2000).

4.1 *Results*

Figures 4 and 5 show effective droplet radius, cloud optical depth, liquid water path and column droplet concentration for April 2 and 5, 1987, respectively.

Recall from Figure 1 that April 2 precedes the incursion of sulfate into the area and that the aerosol layer is well established by April 5. All data are derived from pixels that have passed the spatial coherence screening and have Channel 1 albedo > 0.10. No retrievals are made for droplets having radii > 30 μm; the upper left hand panel of Figure 4 suggests the presence of larger drops (or possibly, ice crystals). The sharp decrease in effective radius and increase in column droplet concentration from April 2 to April 5 are apparent. Evidently enhanced numbers of cloud condensation nuclei have resulted in a much higher column droplet concentration on the day with high sulfate, April 5, than on the day with low sulfate, April 2. The effective droplet radii are correspondingly smaller, with a complete absence of pixels having cloud droplet effective radii > 20 μm. These are the expected signatures of aerosol indirect forcing.

Although the changes in droplet size and number concentration are indicative of an anthropogenic aerosol influence, these changes by themselves do not provide the radiative forcing, which must be manifested in a change in cloud optical depth. For that one must look to LWP and τ on the two days. Unfortunately, the variability in LWP is so great as to mask the variability in τ, so that the differences in optical depths on the two days do not provide a clear picture. Other complications are the fact that the inferred LWP depends not just on the true mean LWP but also on the degree of horizontal inhomogeneity present in the cloud field (Cahalan et al. 1994), and the effect of non-adiabatic processes that could conceivably be different on the two days.

5. CONCLUSIONS

Here we have used the output of a chemistry/transport model to identify a situation in which sulfate aerosol from industrial sources may be expected to exert a strong influence on cloud microphysical and radiative properties in an oceanic area that is well displaced from source regions. Pertinent cloud microphysical properties (optical depth and cloud drop radius) are inferred from radiance data obtained from satellite remote sensing. Comparison of these quantities in situations where the model indicates the presence or absence of industrial sulfate has allowed identification of the expected signature of one aerosol indirect effect – an increase in droplet number concentration and concomitant decrease in droplet radii, on a synoptic scale. Although the information obtained on changes in cloud optical depth is too meager to draw conclusions regarding radiative forcing, there is no doubt that the cloud microphysical properties are influenced by the incursion of continental sulfate aerosol in a way that is consistent with that expected by the Twomey indirect forcing mechanism.

6. ACKNOWLEDGMENTS

We thank Jim Coakley for computer code and advice on the use of the spatial coherence method for AVHRR GAC data and Takashi Nakajima of NASDA/EORC, Japan, for providing us with the retrieval module. This study was partially supported by NASA training grant NGT5-30040 and NASA grant NAG5-7727. Work at BNL was supported also by the Environmental Sciences Division of the U. S. Department of Energy and was performed under Contract No. DE-AC02-98CH10886.

7. REFERENCES

Benkovitz, C.M., and S.E. Schwartz, 1997: Evaluation of modeled sulfate and SO_2 over North America and Europe for four seasonal months in 1986-87. *J. Geophys. Res.*, **102**, 25,305-25,338.

Benkovitz, C.M., C.M. Berkowitz, R.C. Easter, S. Nemesure, R. Wagener, and S.E. Schwartz, 1994: Sulfate over the North Atlantic and adjacent continental regions: Evaluation for October and November 1986 using a three-dimensional model driven by observation-derived meteorology. *J. Geophys. Res.,* **99**, 20,725-20,756.

Benkovitz, C.M., M.A. Miller, S.E. Schwartz, O.-U. Kwon, 2001: The influence of cut-off lows on sulfate burdens over the North Atlantic during April, 1987. *Preprints, A Millennium Symposium on Atmospheric Chemistry, Albuquerque, NM, Amer. Meteor. Soc.*, Paper 7.6 (this volume).

Brenguier, J.-L., H. Pawlowska, L. Schüller, R. Preusker, J. Fischer, and Y. Fouquart, 2000: Radiative properties of boundary layer clouds: Droplet effective radius versus number concentration. *J. Atmos. Sci.,* **57**, 803-821.

Cahalan, R.F., W. Ridgway, W.J. Wiscombe, T.L. Bell, and J.B. Snider, 1994: The albedo of fractal stratocumulus clouds. *J. Atmos. Sci.,* **51**, 2434-2455.

Coakley, J.A., Jr., and F.P. Bretherton, 1982: Cloud cover from high-resolution scanner data: Detecting and allowing for partially filled fields of view. *J. Geophys. Res.*, **87**, 4917-4932.

Coakley, J.A., Jr., and R. Davies, 1986: The effect of cloud sides on reflected solar radiation as deduced from satellite observations. *J. Atmos. Sci.*, **43**, 1025-1035.

Han, Q., W.B. Rossow, and A.A. Lacis, 1994: Near-global survey of effective droplet radii in liquid water clouds using ISCCP data. *J. Climate*, **7**, 465-497.

Han, Q., W.B. Rossow, J. Chou, and R.M. Welch,1998: Global variation of column droplet concentration in low-level clouds. *Geophys. Res. Lett.,* **25**, 1419-1422.

Intergovernmental Panel on Climate Change, 1995: Climate Change 1994: Radiative Forcing of Climate Change, ed. J.T. Houghton et al. *Cambridge University Press*, 339 pp.

Nakajima, T.Y., and T. Nakajima,1995: Wide-area determination of cloud microphysical properties from NOAA AVHRR measurements for FIRE and ASTEX regions. *J. Atmos. Sci.*, **52**, 4043-4059.

Stephens, G.L., 1984: The parameterization of radiation for numerical weather prediction and climate models. *Mon. Wea. Rev.*, **112**, 826-867.

Twomey, S., 1977: The influence of pollution on the short-wave albedo of clouds. *J. Atmos. Sci.*, **34**, 1149-1152.

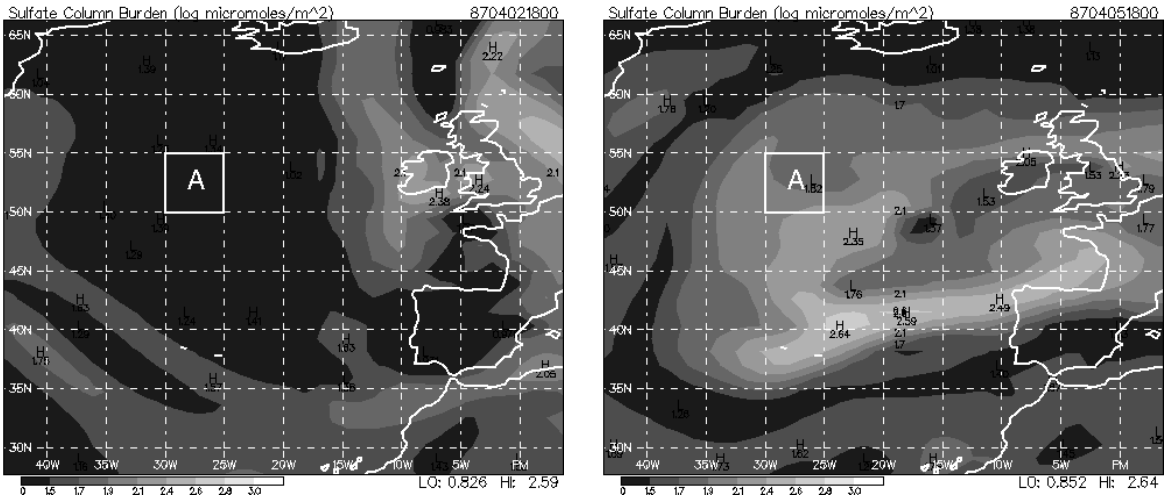

Figure 1. Sulfate column burden in units of $\log_{10}$ micromoles/m^2 as simulated by the BNL GChM-O. The left hand panel is for April 2, 1987 and the right hand panel is for April 5, 1987. Both realizations are at 1800 UTC. The study region is marked A.

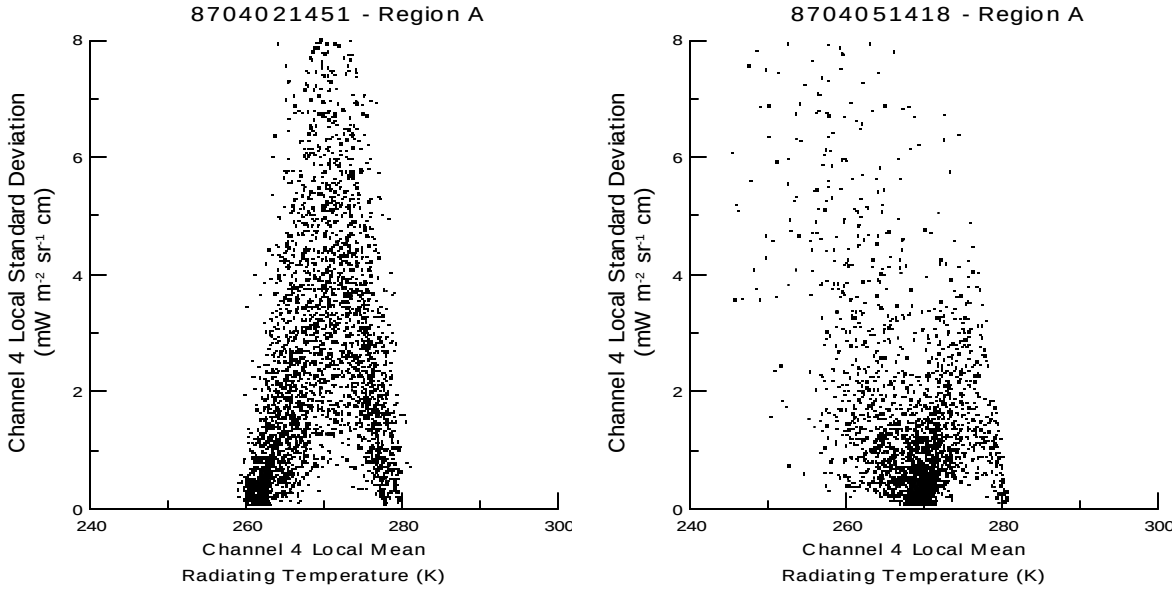

Figure 2. Local means and local standard deviations of AVHRR Channel 4 (11 μm) radiances. The mean radiance is expressed as radiating temperature in Kelvin; the standard deviation is in radiance units (mW m^{-2} sr^{-1} cm). The left hand panel is for April 2, 1987 and the right hand panel is for April 5, 1987. Both are for the region bounded by latitudes 50N and 55N and longitudes 25W and 30W, labeled A in Figure 1.

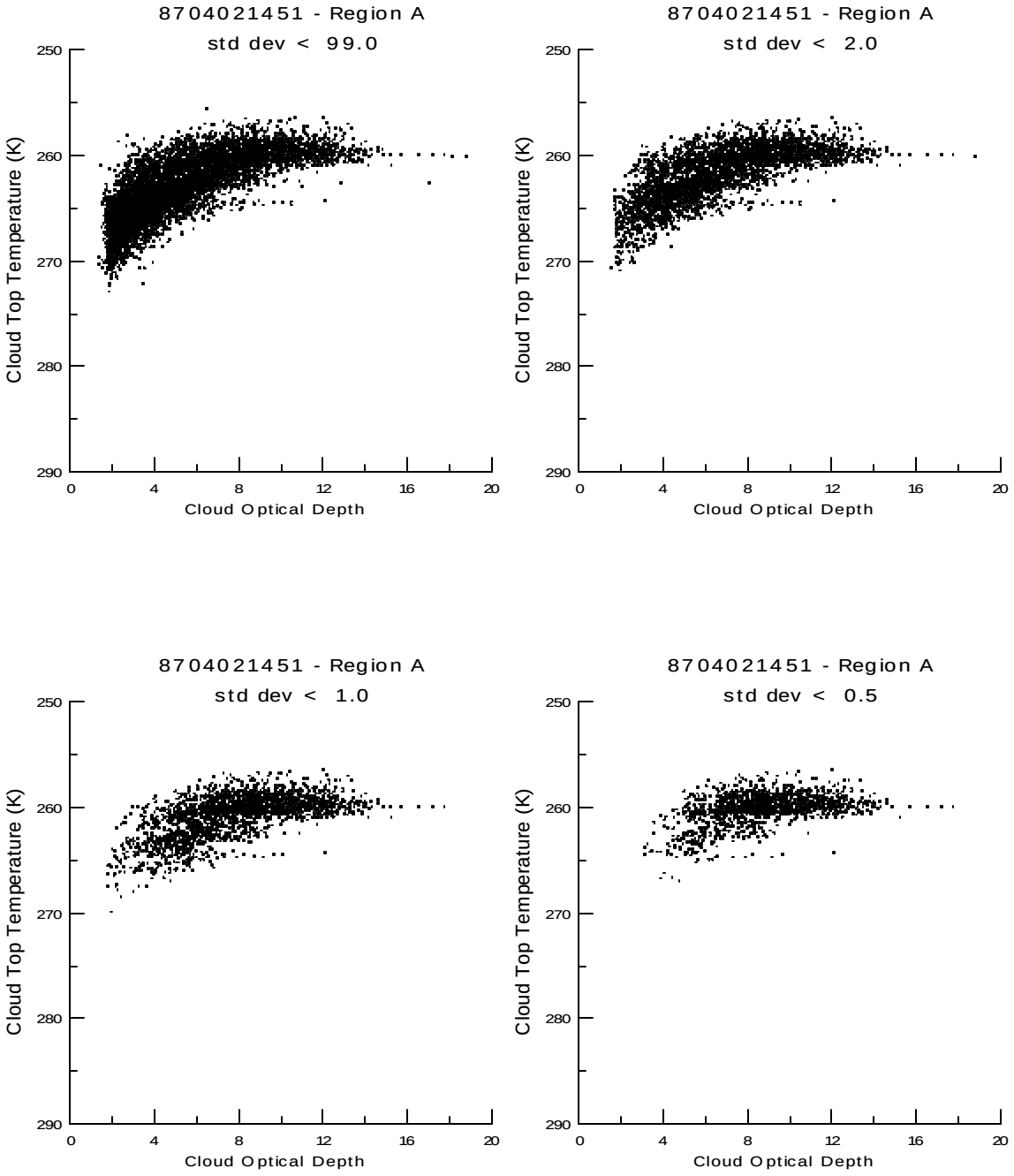

Figure 3. The retrieved cloud optical depth for April 2, 1987, plotted versus the cloud top temperature in Kelvin. Each scatter plot shows pixels that correspond to Channel 4 radiance standard deviation cutoffs of 99.0, 2.0, 1.0, 0.5, respectively, from the left hand panel of Figure 2. Note the progressive screening of partially filled pixels. A Channel 1 reflectance threshold of 0.10 has also been applied.

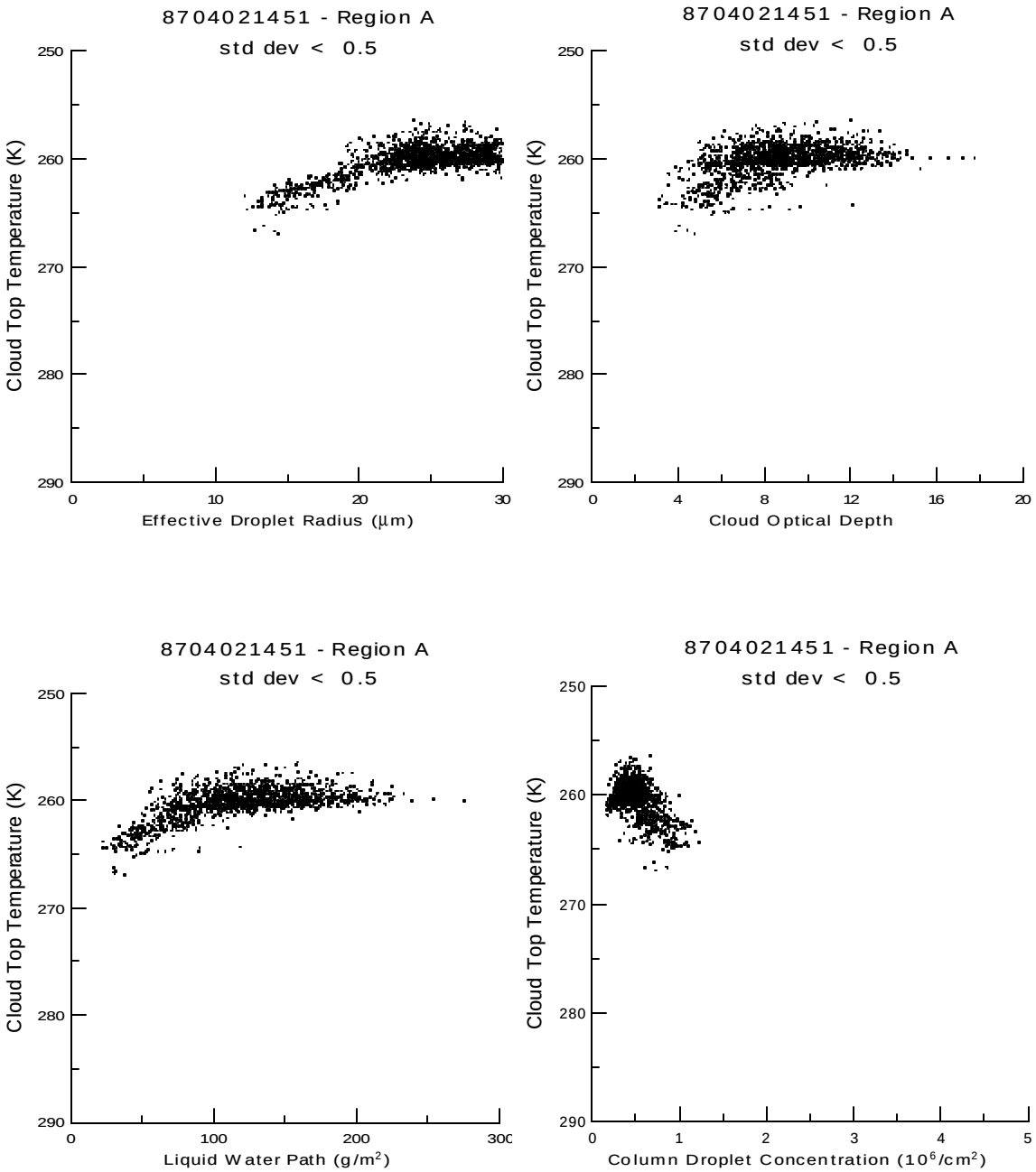

Figure 4. Effective droplet radius, cloud optical depth, liquid water path, and column droplet concentration plotted against the cloud top temperature in Kelvins for all pixels meeting the criterion of Channel 4 local standard deviation < 0.5. Panels are for April 2, 1987 and the region in Figures 2 and 3.

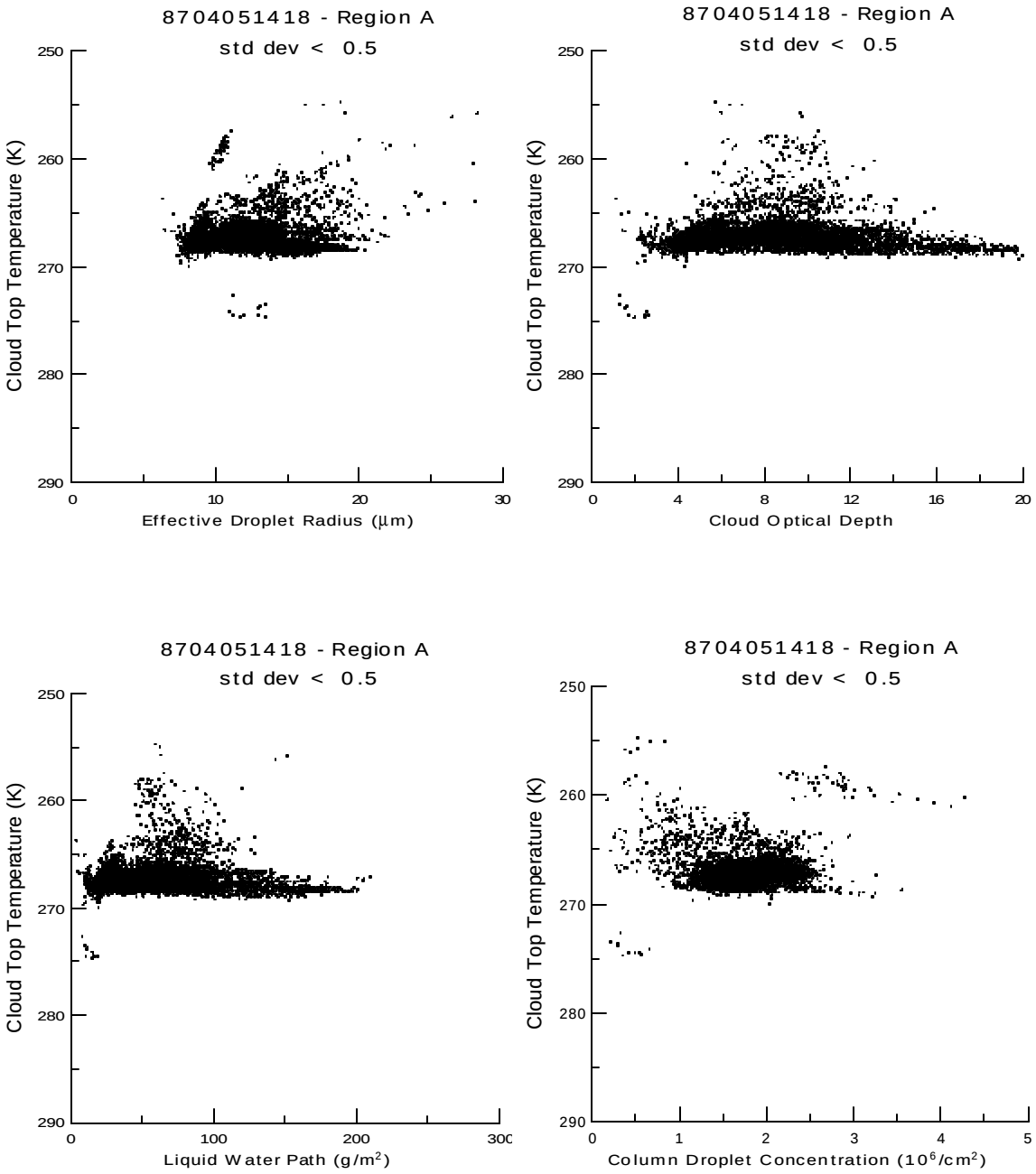

Figure 5. As in Figure 4 but for April 5, 1987.